Nanoscale

PAPER

View Article Online
View Journal | View Issue

Cite this: *Nanoscale*, 2019, **11**, 8994

Structural origin of the high-performance light-emitting InGaN/AlGaN quantum disks†

Shaobo Cheng,[a] Brian Langelier,[a] Yong-Ho Ra,[b] Roksana Tonny Rashid,[b] Zetian Mi[b,c] and Gianluigi A. Botton*[a]

Received 10th February 2019,
Accepted 8th April 2019

DOI: 10.1039/c9nr01262a

rsc.li/nanoscale

Ternary III-nitride-based nanowires with highly efficient light-emitting properties are essential for a broad range of applications. By using the selective area molecular-beam epitaxy method, InGaN/AlGaN quantum disks (QDs) embedded in hexagonal GaN nanowires were successfully grown. With the help of atomic-scale-resolved transmission electron microscopy and atom probe tomography, atomic ordering and other related structural information, such as crystallography and local chemistry, have been unambiguously revealed to provide unique insights into the exceptionally strong photoluminescence enhancements. A boomerang-shaped InGaN/AlGaN QD was identified, and atomic-level 1 : 1 periodic chemical ordering within the boomerang shaped AlGaN layers along the *c*-direction was revealed, confirming the preferential site occupation of Al-atoms. This type of growth provides a strong suppression of the quantum-confined Stark effect and is thus likely a very strong contributor to the exceptional properties. This work therefore enables us to directly establish the key structural elements necessary to understand the exceptionally strong emission exhibited by these materials. Optimization of the configurations of QDs could be an alternative design tool for developing various advanced LED device applications with well-designed structure and desirable optical properties.

Introduction

Highly stable and efficient III-nitride compounds have been intensively studied for many optoelectronic applications, including lighting, display, sensing, and medical treatment.[1–4] The performance of conventional III-nitride light emitters is often deteriorated by the strain-induced polarization fields and the resulting quantum-confined Stark effect (QCSE), leading to a considerable blueshift in emission wavelengths (up to 30 nm) under high power operation.[5,6] To date, there is still no effective way to achieve highly efficient and stable semiconductor light emitters for the green, yellow, and amber colors. To avoid QCSE, growing heteroepitaxial III-nitride films oriented along semipolar and non-polar directions has received considerable attention recently, due to the possibility of reducing, or even eliminating, the spontaneous and strain-induced piezoelectric polarization effects that are inherent to growth in the *c*-axis-oriented system.

During the growth of ternary nitride alloy samples, the atomic ordering always happens, and this effect can have a significant influence on the bandgap, optical properties, and carrier transport properties of the III-N alloys.[7–10] The optical properties of III-N compounds can be strongly influenced by the nearest-neighbor scale distribution fluctuations, due to the exciton localization as their intrinsic property. The spontaneous formation of ordering is still not well-understood due to the sophisticated nature of these growth processes occurring far from equilibrium conditions, but this effect has often been regarded as a kinetically limited growth surface-induced process. Atomic ordering in ternary III-V alloys is not uncommon within thin films grown on various substrates.[11,12] In fact, atomic ordering in InGaN offers an alternative way against large-scale compositional inhomogeneities, which can help achieve high quality nanowires for realizing full wavelength spectrum tunability. It has been found that there is a redshift in the cathodoluminescence of the ordered AlGaN alloys compared with the disordered ones, and researchers justified this phenomenon as the result of the localization of the band edge wave functions in the GaN layer.[8] Previous theoretical studies on AlGaN and InGaN have shown that, in ordered structures, the larger cations prefer to stay at the reduced N-coordination sites, especially for the {1011} pyramidal

[a]*Department of Materials Science and Engineering and Canadian Centre for Electron Microscopy, McMaster University, Main Street West, Hamilton, Ontario, L8S 4M1, Canada. E-mail: gbotton@mcmaster.ca*
[b]*Department of Electrical and Computer Engineering, McGill University, 3480 University Street, Montreal, Quebec H3A 0E9, Canada*
[c]*Department of Electrical Engineering and Computer Science, University of Michigan, 1301 Beal Avenue, Ann Arbor, MI 48109, USA*

†Electronic supplementary information (ESI) available. See DOI: 10.1039/c9nr01262a

microfacets, where the exposed surface has alternating *c*-planes and different N-coordination.[8,12,13] However, it is also believed that the strain plays a crucial role in the alloy stability and thus the origins of the ordering are still controversial.[14] An atomic-resolution scale electron microscopy study on the III-N alloy can help to identify the site positions, the crystallography and the elemental occupancies, which may provide some useful suggestions on the structure optimization strategy for the quantum-well device fabrication.

In this work, InGaN/AlGaN nanowire heterostructures, grown on Al_2O_3 substrates by the molecular beam epitaxy (MBE) method, were investigated using various electron microscopy techniques and atom probe tomography (APT). The structural origin of the extraordinary performance of the nanowires is also explored. The GaN nanowires with AlGaN/InGaN quantum disks (QDs) were grown by the selective area growth method. Selective area growth using a patterned mask is an efficient way to localize the nucleation position of 3D structures. This method could limit the nucleation of Ga adatoms only in the opening apertures and allow a precise control of the size and morphology of the nanowires. The InGaN/AlGaN QDs are incorporated as the active medium. With AlGaN as the barrier, there is a formation of the core–shell structure, in which InGaN is surrounded by an AlGaN shell, because the Al adatom has a smaller migration length than the Ga and In adatoms.[15] It is reported that the large bandgap of AlGaN can improve the carrier injection efficiency significantly by providing a strong carrier confinement effect and also reduce surface carrier recombination.[16] Moreover, the formation of bilayer atomic ordering with 1 : 1 periodicity within AlGaN layers has been observed. Photoluminescence measurements were carried out at room temperature showing the extraordinary properties caused by this structure.

Experimental section

The samples for transmission electron microscopy (TEM) studies and APT were prepared with a Zeiss NVision 40 (Carl Zeiss, Germany) dual-beam focused ion beam (FIB) system. The surface of the TEM sample was cleaned in the low ion accelerating voltage mode. The scanning transmission electron microscopy high angle annular dark field (STEM-HAADF) images were obtained with an FEI Titan TEM operated at 200 kV. The microscope is equipped with a high resolution energy-loss spectrometer (Gatan GIF model 966) with the state-of-the-art K2 Summit direct electron detector camera. The spectrum image and the HAADF images were acquired with a convergence semi-angle of 19 mrad and a GIF collection semi-angle of 20.7 mrad. The dwell time of each pixel for electron energy loss spectroscopy (EELS) mapping was 10 ms for increasing the mapping area and minimizing the beam damage.

For the APT samples, nanowires were sputter-coated with ~200 nm of Ni for protection from the FIB beam, then prepared into needles mounted onto Si posts using established liftout procedures, and sharpened using a 10 kV FIB beam.[27,28] APT experiments were conducted using a LEAP 4000X HR (Cameca Instruments, USA), operated in the laser-pulsing mode (355 nm, 50 fJ, 100 kHz) at a specimen temperature of ~38 K and a target detection rate of 1.0% (0.01 ions per pulse). These evaporation conditions produced a measured Ga^+/Ga^{++} charge-state ratio of 1.25–5.38 in the GaN (outside the QDs) and a measured concentration of 50.7–51.5 at% Ga (balance N). Reconstruction and analysis were performed using the IVAS 3.8.2 software, with spatial calibration obtained using SEM images of the tips prior to analysis, and *d*-spacing measurements along [0001] in GaN.

Results and discussion

Fig. 1A is a top-view scanning electron microscopy (SEM) image for the nanowires grown on the Al_2O_3 substrate. It can

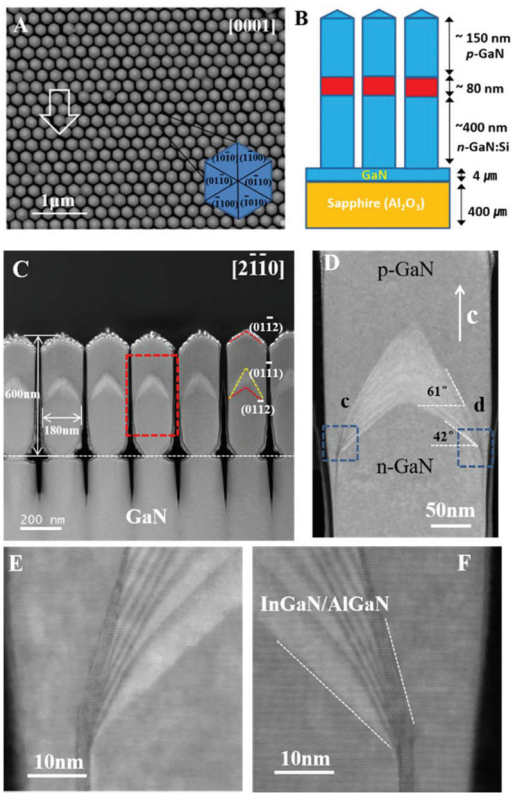

Fig. 1 Basic characterization of the nanowires. (A) A low magnification SEM image showing the top view of the hexagonal pillar structure of the nanowires. The arrow shows the cross-section TEM observation direction. (B) A schematic diagram of the nanowires grown on the sapphire substrate. 8 pairs of InGaN/AlGaN quantum disks are shown in red color. (C) A low magnification HAADF-STEM image for the nanowire from the [2$\bar{1}\bar{1}$0] zone axis. (D) An enlarged image from the red area in (C). The boomerang shaped QDs can be observed. The 42° angle is consistent with the (01$\bar{1}$2) plane and the 61° angle is consistent with the (01$\bar{1}$1) plane. (E) and (F) are magnified from the blue rectangle areas in (D). The QDs with dark intensities are AlGaN and QDs with bright intensities are InGaN.

be observed that the vertically aligned nanowire arrays exhibit a high degree of size uniformity. Careful inspection shows that the top surface of the nanowires has a hexagonal pyramid structure with six facets. The plane indices for the six lateral surfaces are indicated in the inset at the bottom-right corner. The white arrow in Fig. 1A indicates the cross-sectional TEM observation direction. The nanowires with InGaN/AlGaN QDs are schematically illustrated in Fig. 1B. A GaN buffer layer, with a thickness of 4 μm, was firstly grown directly on an Al_2O_3 substrate. Then, n (Si) doped GaN nanowires were grown on the template structure. Eight InGaN/AlGaN QDs were grown at the center of the nanowires subsequently. As shown in Fig. 1B, the repeating growth of the 8 layers of disk-in-a-wire core–shell InGaN/AlGaN QDs allows the formation of relatively uniform shells around the active region and is thus suggested to provide a superior three-dimensional carrier confinement configuration.[17]

Detailed structural characterization of these samples was performed by scanning transmission electron microscopy (STEM). Low magnification high-angle annular dark-field STEM (HAADF-STEM) imaging, providing atomic number contrast information of a single nanowire along the $[2\bar{1}\bar{1}0]$ zone axis, is shown in Fig. 1C and reveals clearly the InGaN/AlGaN QDs in the GaN nanowire. The nanowires have a length of 600 nm and an average diameter of 180 nm. During this bottom-up synthesis process, the efficient surface strain relaxation allows the defects and dislocations within the QDs embedded in the GaN nanowires to be minimized.[6] The overall high crystalline quality of the InGaN/AlGaN heterostructures is demonstrated in Fig. 1D. Rather than a flat horizontal growth of the quantum disks, both InGaN and AlGaN alternating quantum disk layers have hexagonal pyramidal shapes. A detailed view of the active region shows that the InGaN (bright intensity band in the HAADF image) layer is firstly grown epitaxially on the GaN and then capped by another AlGaN (dark intensity band in the HAADF image) barrier, forming a core–shell-like structure at the nanowire sidewall rather than flat alternating quantum disks. The AlGaN shell wrapping the nanowire structure is consistent with previous studies.[17] It has been found that this core–shell structure can improve the efficiency of nanowire LEDs and lasers by minimizing the surface quenching effect and increasing the carrier injection efficiency.[16,18] As shown in Fig. 1D, the starting plane (*i.e.* the eighth QD from the top) and the ending plane for the whole QD stack are 42° ($(01\bar{1}2)$ plane) and 61° ($(01\bar{1}1)$ plane) away from the horizontal *c*-plane, respectively. It is noteworthy to mention that the top surface of the whole GaN nanowire is also a $(01\bar{1}2)$ plane, as shown in Fig. 1C, indicating that the GaN $\{01\bar{1}2\}$ planes have a slower growth speed and are more stable than the $\{01\bar{1}1\}$ planes. For Al doped GaN, the semipolar planes $\{01\bar{1}1\}$ have the slowest growth speed as the QD evolves to grow on such planes, which is consistent with the previous work.[19] The top surface is determined by the slow-growth planes of Al doped GaN, and the bottom surface is determined by the slow-growth planes of pure GaN, which could explain the boomerang shape of the QDs as one end is locked on the same position while the growth in the center of the nanowire is faster to have the growth front evolve from the $(01\bar{1}2)$ plane to the $(01\bar{1}1)$ plane. Fig. 1E and F are high resolution HAADF-STEM images magnified from the blue dashed rectangle areas in Fig. 1D, and all the QDs converge at nearly the same positions at the bottom corners. The InGaN and AlGaN layers are well separated chemically and the interfaces are atomically sharp; thus, the interfacial intermixing is not significant. The nanowires were grown by the MBE method and the chemical potential for the inclined facets is lower than that of the (0001) plane. As discussed by Biasiol *et al.*, the growth is slower along the inclined planes.[20,21] The growth of the nanowire frontier and chemical ordering process can be affected by the competitive nature of the incorporated elements, which can be influenced by their different migration and desorption rates and the supply of atoms to the top of the nanowire during the growth.[12] Among these three elements, In has the highest mobility, while Al has the highest electronegativity and lowest mobility, which also explains the fact that In prefers to accumulate at the growth front.

Since the top of GaN nanowires has a hexagonal pyramidal structure, both InGaN and AlGaN layers should also have similar shapes due to the epitaxy consistency. Therefore, the direction marked by the white arrow in Fig. 1A is the most suitable edge-on observation direction for the QDs. The TEM sample was expected to have uniform thickness, and all the QDs were viewed edge-on. A HAADF-STEM image acquired from the $[10\bar{1}0]$ zone axis (*i.e.* 30° away from the $[2\bar{1}\bar{1}0]$ direction) is shown in Fig. S1A in the ESI.† No contrast from the individual isolated QDs can be found from this $[10\bar{1}0]$ projection, because the QDs are overlapping along this direction. Also, the annular bright-field image (Fig. S1B†) shows that the nanowires are grown along the [0001] direction, which can be denoted as Ga-polar. From these observations, a three-dimensional model for the nanowire with the pyramidal quantum disks can be deduced as shown in Fig. S2.†

Elemental analyses of the nanowires were performed with electron energy loss spectroscopy (EELS) to confirm the chemical origin of the contrast. Elemental maps obtained with the spectrum imaging technique (Fig. 2B–E) illustrate the distribution variation of different elements. The In-map extracted from the In $M_{4,5}$ edge and the Al-map extracted from the Al K edge show the alternating growth of InGaN and AlGaN layers. One should highlight the Al distribution in the AlGaN barrier layers: most of the Al signal is concentrated at the bottom corner and the Al intensity becomes weaker near the top corner of the boomerang-like dots. Moreover, the AlGaN shell is continuous for each AlGaN barrier and is present throughout the whole active region. The formation of such structures can be well explained by the diffusion-controlled growth mechanism of III-nitride nanowires. After impinging on the substrate and side surfaces, the longer diffusion length of Ga and In adatoms, compared to Al, allows them to more easily migrate to the top part of the nanowires and stay, more preferentially, at the growth front, resulting in the growth along the

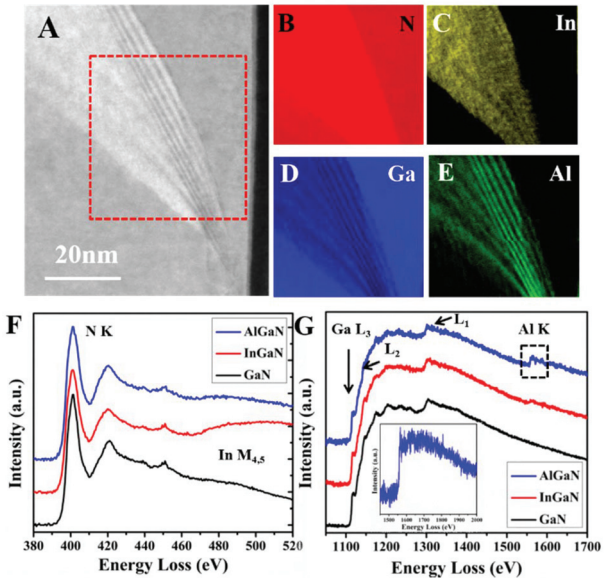

Fig. 2 EELS elemental mapping results for the InGaN/AlGaN QDs. (A) A HAADF-STEM image showing the QD structure at one corner. (B–E) EELS mapping for the N, In, Ga, and Al elemental distributions, respectively. (F) Extracted EELS spectra from the mapping results showing the fine features of N K and In $M_{4,5}$ edges. (G) Extracted EELS spectra for the Ga $L_{1,2,3}$ and Al K edges. The magnified Al K edge can be found in the inset.

axial dimension and the formation of an Al-rich shell on the lateral surface of the nanowire due to the large accumulation of Al atoms near the sidewall.[22] This effect enables the transition of the growth front from the initial $(01\bar{1}2)$ plane to the $(01\bar{1}1)$ plane.

The presence of 8 pairs of InGaN/AlGaN layers is further confirmed by the APT analysis of the nanowires, with results presented in Fig. 3A and B. The 3D structure of the layers is revealed, showing the atomic enrichment of In and Al in the QDs. This InGaN/AlGaN nanowire heterostructure can exhibit superior optical properties in the green spectrum because of the very sharp interfaces and width of the wells. The photoluminescence spectrum measured at room temperature is shown in Fig. 3C. The peak emission wavelength is ~512 nm. The photoluminescence intensity is nearly an order of magnitude stronger, compared to a conventional InGaN/GaN dot-in-nanowire structure measured under identical conditions. The composition measurement is complicated by ion trajectory aberrations in the APT method, but is most reliably measured in the lowest layers, where the layers are largest. Using the bottom 4 QDs, the average In and Al contents are found to be 17.7 ± 1.7 and 9.1 ± 3.1 at%, respectively. This corresponds to an In_xGa_yN stoichiometry with $x = 0.37 \pm 0.05$ and $y = 0.71 \pm 0.04$, which is consistent with the detected wavelength as shown in Fig. 3C based on data shown in ref. 23. The corresponding chemical compositions for Al_xGa_yN are $x = 0.17 \pm 0.06$ and $y = 0.68 \pm 0.04$. The small inhomogeneous broadening of the photoluminescence spectrum could be attributed to the composition variance of the In content shown in Table S1.† The nanowires with a high surface-to-volume ratio grown with this bottom-up approach by MBE enables the release of the residual strain *via* the free surfaces in the sample growth process. The excellent optical properties of the nanowires are also attributed to the absence of dislocations in the InGaN/AlGaN nanostructures, the suppression of non-radiative surface recombination by the atomically ordered AlGaN quantum barrier (with very abrupt interfaces), and the significantly reduced polarization field expected for semipolar InGaN QDs.[24]

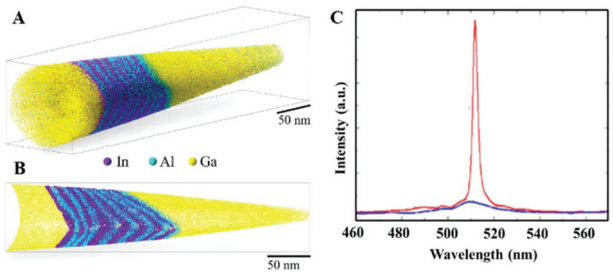

Fig. 3 APT data and the photoluminescence spectrum measurement. The APT data showing In, Al, and Ga, represented as (A) a 3D atom map, and (B) a 10 nm cross-section taken parallel to the long axis of the dataset. The InGaN/AlGaN QDs were revealed by the respective enrichment regions for the In and Al atoms. Note that the field of view limits the APT data to capturing only the volume near the axial centre of the nanowire. (C) A photoluminescence spectrum (red curve) of InGaN/AlGaN dot-in-nanowire structures measured at room temperature. A photoluminescence spectrum (blue curve) of a conventional InGaN/GaN dot-in-nanowire structure measured under identical conditions is also shown for comparison.

Careful inspection of the HAADF images also shows atomic-scale composition fluctuations occurring within the AlGaN layers. What is illustrated in Fig. 4A is a high-magnification HAADF-STEM image showing strongly modulated intensity along the *c*-axis that can be attributed to the local changes in Al concentration. The presence of an extensive atomic-scale Al-rich plane/Al-deficient plane modulation along the growth direction can be clearly observed in Fig. 4B. Such atomic plane scale modulations are too fine to be resolved with APT measurements given the spatial resolution of this technique. Fig. 4C shows the intensity profile along the arrow direction averaged from the blue rectangle area in Fig. 4B. Interestingly, no such ordering occurs in the InGaN layer. Further chemical evidence validating the compositional origin of the observed Z-contrast intensity modulations is provided by EELS mapping carried out at atomic-resolution, which can be found in the ESI.† Intensity line profiles of different elements in Fig. S3E in the ESI† emphasize their unequivocal correspondence between the intensity in the HAADF profiles and the atomically resolved maps of Ga and Al: there are (0001) planes with a lower Ga signal and a corresponding higher Al signal. Fig. 4D and E present the Fourier transform analysis from the blue and yellow squares in Fig. 4A, respectively. The (0001) spot, which is forbidden in GaN, is present in Fig. 4E, indicating that an ordering along the [0001] direction appears in the

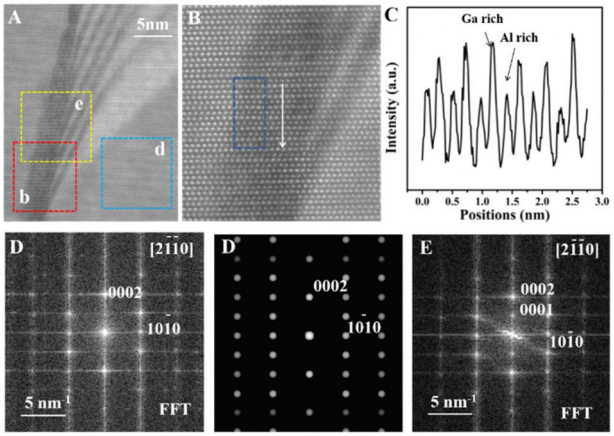

Fig. 4 TEM observations related to the 1 : 1 modulation in the AlGaN layer. (A) A high resolution HAADF-STEM image of one corner of the QDs. (B) An enlarged image from the red rectangle area in (A). (C) The HAADF intensity profile extracted from the dark blue rectangle area along the arrow direction in (B). The intensity modulation can be observed. The atomic layers with brighter intensities are Al-deficient layers, while the layers with relatively dark intensities are Al-rich layers. (D) A fast Fourier transform (FFT) pattern for the light blue boxed area in (A). The (0001) and (000$\bar{1}$) spots are no longer visible because of the systematic extinction. (E) FFT results for the yellow boxed area in (A). The forbidden (0001) and (000$\bar{1}$) superlattice reflections are present, unambiguously confirming the presence of 1 : 1 bilayer atomic ordering within AlGaN. (F) The simulated SAED pattern for GaN, showing the forbidden (0001) and (000$\bar{1}$) spots.

yellow box area in Fig. 4A. The simulated selected area electron diffraction pattern for an ideal GaN crystal is shown in Fig. 4F, and we also confirm that the (0001) diffraction spot is extinct. The formation of this 1 : 1 [0001] ordered structure leads to reduction of the wurtzite lattice symmetry from $P6_3mc$ to $P3m1$.[25]

From both the experimental studies and the theoretical calculations, the ordered AlGaN structure is expected to be thermodynamically unstable.[8] This is due to the uneven strain distribution. Since the covalent radius of Al is slightly smaller than that of Ga, there is a tensile strain in the Al layers and a compressive strain in the Ga layers. In disordered alloys, each layer contains an equal number of Al and Ga atoms, so the net strain becomes small. However, in this case here, the formation process of such a structure is likely related to the preferential occupation of Al and Ga at different lattice positions on the semipolar facets. The 1 : 1 [0001] ordering in AlGaN alloys occurs at the surface steps and is caused by the different coordination of group-III atoms at the step edges. It has been reported that the incorporation of Al atoms at the sites, where three N bonds can be saturated, allows the system energy to reach the minimum value due to the stronger bonding of Al–N than Ga–N.[8] As shown in Fig. 5A, (10$\bar{1}\bar{1}$) planes have N = 3 coordination sites, which are energetically favorable for locating Al atoms. The formation of such a plane is the result of the diffusion of the adatoms to the step edges or vicinal facets for minimizing the system energy.[26] Careful inspection shows that

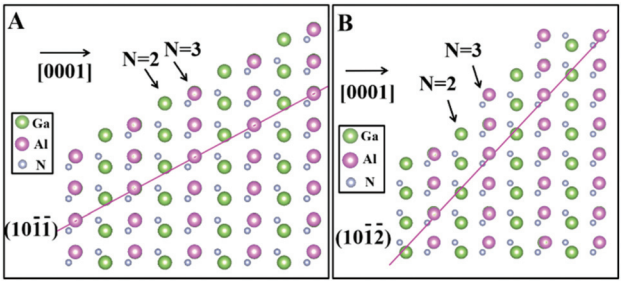

Fig. 5 Schematic diagrams showing the atomic mechanism related to the site occupation. (A) Model of bilayer-ordered AlGaN alloy with Ga-face polarity from the preferential incorporation of Ga at the reduced N-coordination site (2-fold coordinated, N = 2) and Al at the 3-fold coordinated site (N = 3) along a (10$\bar{1}\bar{1}$) surface facet. (B) A model of a bilayer-ordered AlGaN alloy along a (10$\bar{1}\bar{2}$) surface facet.

N = 3 coordination sites also exist on the (10$\bar{1}\bar{2}$) planes as shown in Fig. 5B, which can help explain our experimental observations. Here, although both AlGaN and InGaN layers were grown on the inclined surfaces, the ordering only happened in the AlGaN layer rather than in the InGaN layer.

Conclusions

In summary, with the help of transmission electron microscopy, atom probe tomography and photoluminescence measurements, the structure–property relationship within a InGaN/AlGaN nanowire was explored. Atomic scale chemical ordering in AlGaN alloys in InGaN/AlGaN nanowire heterostructures was systematically studied. The presence of 1 : 1 atomic ordering along the [0001] direction within the AlGaN layer can be clearly revealed from both HAADF-STEM images and atomically resolved EELS results. The preferential site occupation validates the existing theoretical model based on surface site energetics. The ordering only happens in the AlGaN layer rather than in the InGaN layer, indicating AlGaN is more likely to have a surface energetics-induced origin. Moreover, the AlGaN and InGaN layers were grown in alternating sequence, forming three-dimensional boomerang-shaped wells. This unique structure could effectively suppress non-radiative recombination on the lateral surfaces of the active region and, at the same time, reduce quantum confined Stark effects due to the extensive growth on semipolar planes. The metal–organic chemical vapour deposition method can also be used to grow similar structures, which could be more industrially scalable, but potential incorporation issues might need to be overcome to achieve exactly the same architecture. Our results could inspire new strategies for the structure designs for high performance ternary III-nitride compounds.

Conflicts of interest

The authors declare no competing financial interests.

Acknowledgements

G. A. B and S. C. are grateful to NSERC for a Discovery Grant partially supporting this work. G. A. B. and Z. M. acknowledge partial support from a Strategic Project Grant. Z. M. would like to acknowledge National Science Foundation (Grant ECCS-1709207). Electron microscopy was carried out at the Canadian Centre for Electron Microscopy (CCEM), a national facility supported by NSERC, the Canada Foundation for Innovation, under the MSI program, and McMaster University.

Notes and references

1 E. Schubert and J. K. Kim, *Science*, 2005, **308**, 1274–1278.
2 M. K. Choi, J. Yang, K. Kang, D. C. Kim, C. Choi, C. Park, S. J. Kim, S. I. Chae, T. H. Kim, J. H. Kim, T. Hyeon and D. H. Kim, *Nat. Commun.*, 2015, **6**, 7149.
3 S. Nakamura, T. Mukai and M. Senoh, *J. Appl. Phys.*, 1994, **76**, 8189–8191.
4 X. Li, M. Sun, X. Wei, C. Shan and Q. Chen, *Nanomaterials*, 2018, **8**, 188.
5 C.-F. Huang, C.-Y. Chen, C.-F. Lu and C. C. Yang, *Appl. Phys. Lett.*, 2007, **91**, 051121.
6 Y.-H. Ra, R. T. Rashid, X. Liu, J. Lee and Z. Mi, *Adv. Funct. Mater.*, 2017, **27**, 1702364.
7 I. Gorczyca, K. Skrobas, T. Suski, N. E. Christensen and A. Svane, *J. Appl. Phys.*, 2013, **114**, 223102.
8 M. Albrecht, L. Lymperakis, J. Neugebauer, J. E. Northrup, L. Kirste, M. Leroux, I. Grzegory, S. Porowski and H. P. Strunk, *Phys. Rev. B: Condens. Matter Mater. Phys.*, 2005, **71**, 035314.
9 A. Al-Yacoub and L. Bellaiche, *Appl. Phys. Lett.*, 2001, **79**, 2166.
10 X. Li, M. Sun, C. Shan, Q. Chen and X. Wei, *Adv. Mater. Interfaces*, 2018, **5**, 1701246.
11 M. Benamara, L. Kirste, M. Albrecht, K. W. Benz and H. P. Strunk, *Appl. Phys. Lett.*, 2003, **82**, 547.
12 S. Y. Woo, M. Bugnet, H. P. T. Nguyen, Z. Mi and G. A. Botton, *Nano Lett.*, 2015, **15**, 6413–6418.
13 J. E. Northrup, L. T. Romano and J. Neugebauer, *Appl. Phys. Lett.*, 1999, **74**, 2319.
14 C. Tessarek, S. Figge, T. Aschenbrenner, S. Bley, A. Rosenauer, M. Seyfried, J. Kalden, K. Sebald, J. Gutowski and D. Hommel, *Phys. Rev. B: Condens. Matter Mater. Phys.*, 2011, **83**, 115316.
15 Z. Mi, Y. Ra, R. Wang and R. Rashid, *2017 IEEE Photonics Conference (IPC)*, Orlando, FL, 2017, pp. 57.
16 H. P. T. Nguyen, S. Zhang, A. T. Connie, M. G. Kibria, Q. Wang, I. Shih and Z. Mi, *Nano Lett.*, 2013, **13**, 5437–5442.
17 H. P. T. Nguyen, M. Djavid, S. Y. Woo, X. Liu, A. T. Connie, S. M. Sadaf, Q. Wang, G. A. Botton, I. Shih and Z. Mi, *Sci. Rep.*, 2015, **5**, 7744.
18 S. Zhang, A. T. Connie, D. A. Laleyan, H. P. T. Nguyen, Q. Wang, J. Song, I. Shih and Z. Mi, *IEEE J. Quantum Electron.*, 2014, **50**, 483–490.
19 Y. Tian, J. Yan, Y. Zhang, Y. Zhang, X. Chen, Y. Guo, J. Wang and J. Li, *Nanoscale*, 2016, **8**, 11012–11018.
20 G. Biasiol and E. Kapon, *Phys. Rev. Lett.*, 1998, **81**, 2962–2965.
21 G. Biasiol, A. Gustafsson, K. Leifer and E. Kapon, *Phys. Rev. B: Condens. Matter Mater. Phys.*, 2002, **65**, 205306.
22 S. Zhao, S. Y. Woo, M. Bugnet, X. Liu, J. Kang, G. A. Botton and Z. Mi, *Nano Lett.*, 2015, **15**, 7801–7807.
23 S. Y. Woo, N. Gauquelin, H. P. T. Nguyen, Z. Mi and G. A. Botton, *Nanotechnology*, 2015, **26**, 344002.
24 A. Strittmatter, J. E. Northrup, N. M. Johnson, M. V. Kisin, P. Spiberg, H. EI-Ghoroury, A. Usikov and A. Syrkin, *Phys. Status Solidi B*, 2010, **248**, 561–573.
25 P. Ruterana, G. De Saint Jores, M. Laugt, F. Omnes and E. Bellet-Amalric, *Appl. Phys. Lett.*, 2001, **78**, 344.
26 M. Benamara, L. Kirste, M. Albrecht, K. W. Benz and H. P. Strunk, *Appl. Phys. Lett.*, 2003, **82**, 547.
27 D. J. Larson, D. T. Foord, A. K. Petford-Long, H. Liew, M. G. Blamire, A. Cerezo and G. D. W. Smith, *Ultramicroscopy*, 1999, **79**, 287–293.
28 K. Thompson, D. Lawrence, D. J. Larson, J. D. Olson, T. F. Kelly and B. Gorman, *Ultramicroscopy*, 2007, **107**, 131–139.